Journal of Organometallic Chemistry 693 (2008) 3907–3914

Contents lists available at ScienceDirect

Journal of Organometallic Chemistry

journal homepage: www.elsevier.com/locate/jorganchem

Synthesis, characterization, and coordination chemistry of two new tartaric acid-derived bis(phosphite) ligands

Samuel B. Owens Jr., Gary M. Gray *

Department of Chemistry, University of Alabama at Birmingham, 901 14th Street South, Birmingham, AL 35294-1240, United States

ARTICLE INFO

Article history:
Received 24 July 2008
Received in revised form 1 October 2008
Accepted 2 October 2008
Available online 8 October 2008

Keywords:
Tartrates
Molybenum
Platinum
Palladium
Crystal structures
Phosphites

ABSTRACT

The syntheses of two chiral bis(phosphite) ligands with tartaric acid-derived backbones: **1** (from dimethyl tartrate) and **2** (from dipyrollidene tartramide), three complexes of **1**: *cis*-$Mo(CO)_4$(**1**), *cis*-$PtCl_2$(**1**), and *cis*-$PdCl_2$(**1**) and two complexes of **2**: *cis*-$Mo(CO)_4$(**2**) and *cis*-$PdCl_2$(**2**) are described. Each ligand and complex has been fully characterized by ^1H, ^{13}C, and ^{31}P NMR spectroscopy, and the coordination ^{31}P NMR chemical shifts have been compared to those observed for complexes of related ligands. The X-ray crystal structures of each of the metal complexes have also been determined. The X-ray crystal structures indicate that the conformation of the seven-membered chelate ring varies depending on the substituents on the tartrate backbone. However, the conformations of the seven-membered rings do not change when the metal center is changed or when the coordination environment around the metal center is changed.

1. Introduction

Tartaric acid derivatives are readily available and enantiomerically pure diols that have been used for the preparation of a variety of chiral bis(phosphorous-donor) ligands for use in enantioselective catalysis. Dang and Kagan prepared the earliest of these ligands, DIOP, in 1971, in which the tartaric acid derivative formed the backbone of the bis(phosphine) ligand [1]. More recently, van Leeuwen et al. [2] have prepared a number of bis(phosphites) via the reactions of chlorophosphites with tartaric acid-derived diols. The tartaric acid derivatives form the backbones of these ligands. Kwok and Wink [3] have taken a slightly different approach by reacting tartrate esters with phosphorus trichloride to form 2-chloro-1,3-dioxapholanes (chlorophosphites). These intermediates were then reacted with diols to form bis(1,3,2-dioxaphospholane) ligands. In these ligands, the tartaric acid derivatives are incorporated as substituents of the phosphorus-donor groups rather than as the backbones of the ligand.

To date, the research involving bis(phosphite) ligands derived from tartaric acid has focused on their catalytic activities and selectivities. In contrast, the coordination chemistry of these ligands has not been investigated. Studying the coordination chemistry may provide insights into the geometries adopted by the ligands in the octahedral and square planar intermediates in the catalytic cycles. These insights, in turn, may suggest modifications to the structures of the ligands that would improve the catalytic activities and selectivities of their transition metal complexes.

In this manuscript, we report the synthesis of both octahedral *cis*-$Mo(CO)_4L$ and square planar *cis*-MCl_2L (M = Pd(II), Pt(II)) complexes of two bis(phosphite) ligands similar to those reported by van Leeuwen. The X-ray crystal structures of each of the complexes have been determined. These structures have been compared to better understand the factors that affect the conformations of the ligands in their transition metal complexes.

2. Experimental

2.1. Materials and characterization

All reactions were carried out under a dry N_2 atmosphere using the appropriate Schlenk glassware and techniques. Both THF and Et_3N were obtained from Aldrich and dried by distillation from sodium benzophenone ketyl. Dimethyl tartrate was purchased from Aldrich and azeotropically dried from toluene. The dipyrrolidine tartramide was synthesized from a known literature procedure [4]. The 2-chloro-5,5-dimethyl-1,3,2-dioxaphosphorinane [5], $PtCl_2$(cod) [6], $PdCl_2(MeCN)_2$ [7], and $Mo(CO)_4$(nbd) [8,9] were prepared by literature methods. $PdCl_2$ was obtained from Pressure Chemical Co. and used without further purification. All NMR spectra were recorded on a Bruker DRX400 spectrometer. The chloroform-*d* solvent was obtained from Cambridge Isotopes and opened and handled under N_2. The $^{31}P\{^1H\}$ NMR spectra were referenced to external 85% phosphoric acid, and both the ^{13}C and the

* Corresponding author. Tel.: +1 205 934 8094; fax: +1 205 934 2543.
E-mail address: gmgray@uab.edu (G.M. Gray).

0022-328X/$ - see front matter © 2008 Elsevier B.V. All rights reserved.
doi:10.1016/j.jorganchem.2008.10.003

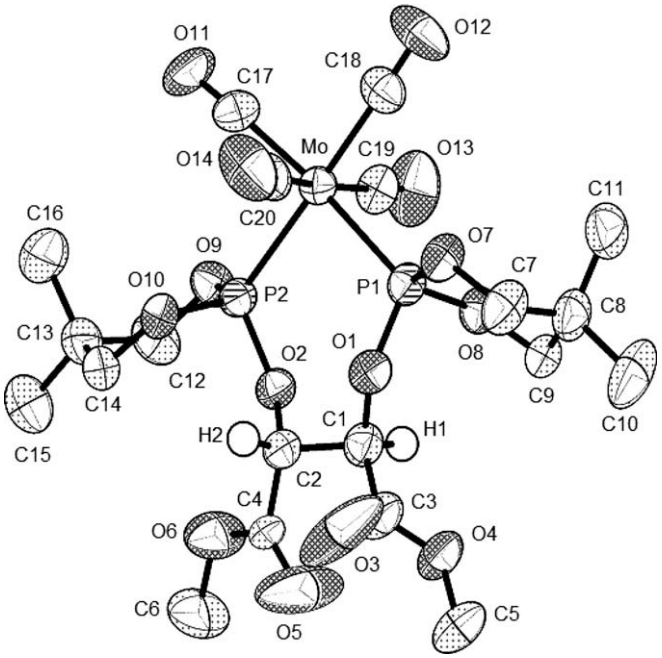

Fig. 1. ORTEP [19] drawing of the molecular structure of **3**. Thermal ellipsoids are drawn at the 50% probability level and hydrogens in calculated positions are omitted for clarity.

^{1}H NMR spectra were referenced to internal $SiMe_4$. IR spectra were taken of CH_2Cl_2 solutions of the complexes in NaCl solution cells on a Bruker Vertex 70 FT IR spectrometer.

2.2. X-ray data collection and solution

Suitable single crystals of **3–7** were glued on glass fibers with epoxy and aligned upon an Enraf-Nonius CAD4 single-crystal Diffractometer under aerobic conditions. Standard peak search and automatic indexing routines followed by least-squares fits of 25 accurately centered reflections resulted in accurate unit cell parameters for each. The space groups of the crystals were assigned on the basis of systematic absences and intensity statistics. All data collections were carried out using the CAD4-PC software [10], and details of the data collections are given in Tables 1 and 2. The analytical scattering factors of the compounds were corrected for

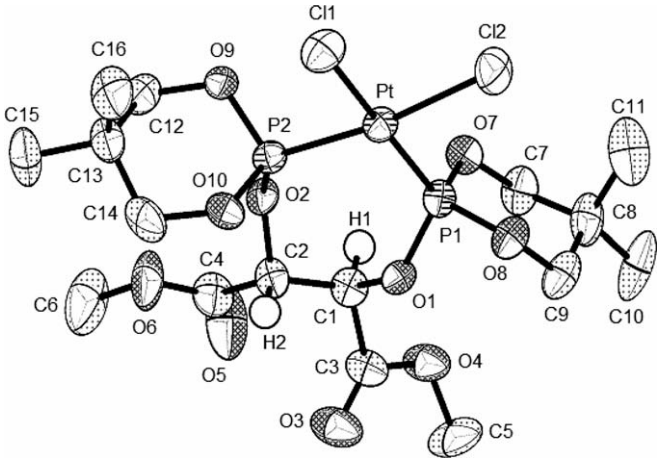

Fig. 2. ORTEP [19] drawing of the molecular structure of **4**. Thermal ellipsoids are drawn at the 50% probability level and hydrogens in calculated positions are omitted for clarity.

both $\Delta f'$ and $i\Delta f''$ components of anomalous dispersion. All data were corrected for Lorentz and polarization effects, and empirical absorption corrections were applied when necessary. All crystallographic calculations were performed with the Siemens SHELXTL-PC program package [11]. The Mo, Pd, Pt and P positions were located using the Patterson method, and the remainder of the non-hydrogen atoms were located in difference Fourier maps. Full-matrix refinements of the positional and anisotropic thermal parameters for all non-hydrogen atoms versus F^2 were carried out. All hydrogen atoms were placed in calculated positions with the appropriate molecular geometry and d(C–H) = 0.96 Å. The isotropic thermal parameter of each hydrogen atom was fixed equal to 1.2 times the U_{eq} value of the atom to which it was bound. Selected bond lengths and angles for **3–7** are given in Tables 3 and 4, and ORTEP drawings of the compounds are shown in Figs. 1–5. Crystallographic data for complexes **3–7** have been deposited with the Cambridge Crystallographic Database (CCDCs: 691447–691451).

*(2R,3R)-Bis-(5,5-dimethyl-[1,3,2]dioxaphosphinan-2-yloxy)-succinic acid dimethyl ester (**1**).* A 250 mL round bottom flask was charged with 1.07 g (6.00 mmol) of the (2R,3R)-dimethyl tartrate, 1.21 g (12.0 mmol) dry Et_3N and 100 mL of dry THF. Then, a solution of 2.00 g (12.0 mmol) of 2-chloro-5,5-dimethyl-1,3,2-dioxaphosphorinane in 40 mL of THF was added dropwise with stirring over a period of 30 min, causing a white precipitate to form. The solution was stirred for an additional 30 min and then was filtered through a 1 cm bed of Celite in a 60 cc medium sintered glass funnel under nitrogen. The resulting filtrate was evaporated to dryness to yield 2.30 g (86.8%) of **1** as a white solid. ^{31}P{^{1}H} NMR ($CDCl_3$): δ 123.14 (s). ^{1}H NMR ($CDCl_3$): δ 5.02 (dd, 2 H, $|^2J$(PH)| 7.5 Hz, $|^3J$(HH)| 2.9 Hz, C*H*), 4.25 (dd, 2H, $|^3J$(PH)| 10.3 Hz, $|^3J$(HH)| 2.7 Hz, CH_2O), 4.12 (dd, 2H, $|^3J$(PH)| 10.3 Hz, $|^3J$(HH)| 2.7 Hz, CH_2O), 3.72 (s, 6H, OCH_3), 3.26 (m, 4H, CH_2O), 1.17 (s, 6H, CCH_3), 0.67 (s, 6H, CCH_3). ^{13}C{^{1}H} NMR ($CDCl_3$): δ 167.92 (s, *C*=O), 75.11 (s, *C*H), 72.79 (s, *C*H_2O), 72.55 (s, *C*H_2O), 51.57 (s,O*C*H_3), 31.62 (s, *C*CH_3), 21.71 (s, C*C*H_3), 21.41 (s, CCH_3).

*(2R,3R)-Bis-(5,5-dimethyl-[1,3,2]dioxaphosphinan-2-yloxy)-1,4-dipyrrolidine-1-yl-butane-1,4-dione (**2**).* A 250 mL round bottom flask was charged with 1.54 g (6.00 mmol) of the 1,1′-[(2R,3R)-2,3-dihydroxy-1,4-dioxo-1,4-butanediyl]bis-pyrrolidene [4], 1.21 g (12.0 mmol) dry Et_3N and 100 mL of dry THF. Then, a solution of 2.00 g (12.0 mmol) of 2-chloro-5,5-dimethyl-1,3,2-dioxaphosphorinane in 40 mL of THF was added dropwise with stirring over a period of 30 min, causing a white precipitate to form. The solution was stirred for an additional 30 min and then was filtered through a 1 cm bed of Celite in a 60 cc medium sintered glass funnel under nitrogen. The resulting filtrate was evaporated to dryness to yield 2.63 g (84.3%) of **2** as a white solid. ^{31}P{^{1}H} NMR ($CDCl_3$): δ 124.03 (s). ^{1}H NMR ($CDCl_3$): δ 5.51 (dd, 2H, $|^3J$(HH)| 7.5 Hz, $|^3J$(PH)| 7.5 Hz C*H*), 3.95 (t, 4H, $|^4J$(HH)| 2.8 Hz, CH_2O), 3.74 (t, 4H, $|^4J$(HH)| 2.8 Hz, CH_2O), 3.45 (m, 8H, CH_2N), 1.91 (m, 8H, CH_2C), 1.30 (s, 6H, CH_3C), 0.73 (s, 6H, CH_3C). ^{13}C{^{1}H} NMR ($CDCl_3$): δ 165.88 (s, *C*=O), 73.25 (s, *C*H_2O), 73.11 (s, *C*H), 72.37 (s, *C*H_2O) 46.38 (s, *C*H_2N), 45.78 (s, *C*H_2N), 32.11 (s, *C*CH_3), 26.11 (s, *C*H_2C), 24.35 (s, *C*H_2C) 22.12 (s, C*C*H_3), 22.00 (s, CCH_3) (see Fig. 3).

*cis-Mo(CO)$_4$(**1**) (**3**).* To a 100 mL round bottom flask was added 0.30 g (1.0 mmol) of Mo(CO)$_4$(nbd) and 50 mL of degassed CH_2Cl_2. This solution was stirred until all of the Mo(CO)$_4$(nbd) had dissolved at which time 0.50 g (1.0 mmol) of **1** was added in one portion. The reaction mixture was stirred for 30 min resulting in a pale yellow solution. A ^{31}P{^{1}H}NMR spectrum of the reaction mixture was then taken and exhibited the single resonance of the product. The mixture was evaporated to dryness under aspirator vacuum, and the residue was placed on the pump to insure removal of all excess norbornadiene and solvent. The resulting dark yellow solid was taken up in CH_2Cl_2, and the solution was run through a ~1 cm

Table 1
Crystal data and structure refinement for compounds **3**, **4**, and **5**.

	3	**4**	**5**
CCDC #	691447	691448	691449
Empirical formula	C_{20} H_{28} Mo O_{14} P_2	C_{16} H_{28} Cl_2 O_{10} P_2 Pt	C_{16} H_{28} Cl_2 O_{10} P_2 Pd
Formula weight	650.30	708.31	619.62
Temperature (K)	293(2)	293(2)	293(2)
Wavelength (Å)	0.71073	0.71073	0.71073
Crystal system	Orthorhombic	Orthorhombic	Orthorhombic
Space group	$P2_12_12_1$	$P2_12_12_1$	$P2_12_12_1$
Unit cell dimensions			
a (Å)	10.093(2)	10.281(2)	10.296(2)
b (Å)	15.493(3)	10.466(2)	10.427(2)
c (Å)	17.760(4)	23.265(5)	23.222(5)
α, β, γ (°)	90, 90, 90	90, 90, 90	90, 90, 90
Volume (Å^3)	2777.2(10)	2503.4(9)	2493.0(9)
Z	4	4	4
Density (calculated) (mg/m^3)	1.555	1.879	1.651
Absorption coefficient (mm^{-1})	0.651	5.992	1.133
F(000)	1328	1384	1256
Crystal size (mm^3)	0.16 × 0.60 × 0.50	0.17 × 0.10 × 0.46	0.48 × 0.36 × 0.28
θ range for data collection (°)	2.29–22.47	2.13–22.47	2.14–22.48
Index ranges	$0 \leqslant h \leqslant 10$, $-16 \leqslant k \leqslant 16$, $-1 \leqslant l \leqslant 19$	$0 \leqslant h \leqslant 11$, $0 \leqslant k \leqslant 11$, $-25 \leqslant l \leqslant 25$	$-11 \leqslant h \leqslant 0$, $-1 \leqslant k \leqslant 11$, $-1 \leqslant l \leqslant 24$
Reflections collected	4276	3679	2230
Independent reflections [$R_{(int)}$]	3614 [0.0172]	3263 [0.0273]	2150 [0.0242]
Completeness to θ = 22.47° (%)	100.0	99.9	99.9
Absorption correction	Empirical	Empirical	Empirical
Refinement method	Full-matrix least-squares on F^2	Full-matrix least-squares on F^2	Full-matrix least-squares on F^2
Data/restraints/parameters	3614/0/341	3263/0/288	2150/0/287
Goodness-of-fit (GOF) on F^2	1.078	1.033	1.093
Final R indices [$I > 2\sigma(I)$]	R_1 = 0.0294, wR_2 = 0.0719	R_1 = 0.0321, wR_2 = 0.0772	R_1 = 0.0271, wR_2 = 0.0661
R indices (all data)	R_1 = 0.0356, wR_2 = 0.0748	R_1 = 0.0392, wR_2 = 0.0805	R_1 = 0.0324, wR_2 = 0.0684
Largest difference peak and hole (e Å^{-3})	0.397 and −0.359	0.804 and −0.556	0.359 and −0.409

Table 2
Crystal data and structure refinement for compounds **6** and **7**.

	6	**7**
CCDC #	691450	691451
Empirical formula	C_{27} H_{40} Cl_2 Mo N_2 O_{12} P_2	C_{22} H_{38} Cl_2 N_2 O_9 P_2 Pd
Formula weight	813.39	713.78
Temperature (K)	293(2)	293(2)
Wavelength (Å)	0.71073	0.71073
Crystal system	Monoclinic	Orthorhombic
Space group	$P2_1$	$P2_12_12_1$
Unit cell dimensions		
a (Å)	10.620(2)	8.9028(18)
b (Å)	11.245(2)	14.899(3)
c (Å)	15.381(3)	24.378(5)
α (°)	90	90
β (°)	91.69(3)	90
γ (°)	90	90
Volume (Å^3)	1836.0(6)	3233.6(11)
Z	2	4
Density (calculated) (mg/m^3)	1.471	1.466
Absorption coefficient (mm^{-1})	0.647	0.884
F(000)	836	1464
Crystal size (mm^3)	0.14 × 0.26 × 0.34	0.18 × 0.12 × 0.34
θ range for data collection (°)	2.24–22.48	2.16–22.47
Index ranges	$-1 \leqslant h \leqslant 11$, $-12 \leqslant k \leqslant 0$, $-16 \leqslant l \leqslant 16$	$0 \leqslant h \leqslant 9$, $-16 \leqslant k \leqslant 0$, $-26 \leqslant l \leqslant 1$
Reflections collected	3038	2545
Independent reflections [$R_{(int)}$]	2551 [0.0209]	2521 [0.0358]
Completeness to θ = 22.47° (%)	99.9	99.9
Absorption correction	Empirical	None
Refinement method	Full-matrix least-squares on F^2	Full-matrix least-squares on F^2
Data/restraints/parameters	2551/1/421	2521/0/348
Goodness-of-fit (GOF) on F^2	1.046	1.024
Final R indices [$I > 2\sigma(I)$]	R_1 = 0.0384, wR_2 = 0.0989	R_1 = 0.0519, wR_2 = 0.1252
R indices (all data)	R_1 = 0.0493, wR_2 = 0.1068	R_1 = 0.0912, wR_2 = 0.1420
Largest difference peak and hole (e Å^{-3})	0.451 and −0.543	0.640 and −0.498

thick pad of silica gel in a 15 cc medium sintered glass funnel under nitrogen. This colorless solution was again evaporated to dryness to yield under aspirator vacuum and then under high vacuum to yield 0.64 g (98%) of crude **3** as a white solid. The crude product was recrystallized from CH_2Cl_2/hexanes to yield colorless X-ray quality crystals. Anal. Calc. for $C_{20}H_{28}O_{14}P_2Mo$: C, 36.94; H,

Table 3
Selected bond lengths (Å) and bond angles (°) for compounds **3** and **6**.

	3	6
M–P(1)	2.4213(13)	2.438(2)
M–P(2)	2.4299(13)	2.401(2)
O(1)–P(1)	1.629(3)	1.634(6)
O(2)–P(2)	1.633(3)	1.627(5)
C(1)–O(1)	1.426(6)	1.455(9)
C(1)–C(2)	1.538(7)	1.494(11)
C(2)–O(2)	1.424(6)	1.434(9)
C(23)–Mo	2.029(6)	2.020(9)
C(24)–Mo	1.983(5)	2.033(9)
C(25)–Mo	2.029(6)	2.016(15)
C(26)–Mo	2.046(6)	2.047(15)
C(23)–O(9)	1.136(6)	1.132(10)
C(24)–O(10)	1.158(6)	1.128(10)
C(25)–O(11)	1.127(6)	1.151(18)
C(26)–O(12)	1.127(6)	1.112(18)
P(1)–M–P(2)	89.83(4)	93.53(7)
O(1)–P(1)–M	116.75(12)	122.5(2)
C(1)–O(1)–P(1)	126.6(3)	127.4(5)
O(1)–C(1)–C(2)	109.6(4)	114.2(6)
O(2)–C(2)–C(1)	108.5(4)	108.8(7)
C(2)–O(2)–P(2)	125.3(3)	119.3(5)
O(2)–P(2)–M	119.29(12)	118.7(2)
C(3)–C(1)–C(2)	111.8(4)	110.7(8)
C(4)–C(2)–C(1)	111.7(4)	109.0(6)
O(9)–C(23)–Mo	177.6(5)	177.3(14)
O(10)–C(24)–Mo	178.1(5)	177.4(18)
O(11)–C(25)–Mo	176.2(5)	178.5(12)
O(12)–C(26)–Mo	174.5(5)	178.7(13)
C(24)–Mo–P(1)	93.46(16)	86.5(2)
C(25)–Mo–P(1)	89.71(15)	88.5(3)
C(26)–Mo–P(1)	87.08(17)	88.1(4)
C(23)–Mo–P(2)	85.28(14)	87.1(2)
C(24)–Mo–P(2)	174.62(15)	178.7(5)
C(25)–Mo–P(2)	88.83(15)	89.2(4)
C(26)–Mo–P(2)	97.19(15)	91.2(3)

4.34. Found: 37.07; H, 4.39%. ^{31}P NMR ($CDCl_3$): δ 154.68 (s). ^{1}H NMR ($CDCl_3$): δ 5.02 (dd, 2H, $|^2J(PH)|$ 7.5 Hz, $|^3J(HH)|$ 2.9 Hz C*H*), 4.25 (dd, 2H, $|^3J(PH)|$ 10.3 Hz, $|^3J(HH)|$ 2.7 Hz, CH_2O), 4.12 (dd, 2H, $|^3J(PH)|$ 10.3 Hz, $|^3J(HH)|$ 2.7 Hz, CH_2O), 3.72 (s, 6H, OCH_3), 3.26 (m, 4H, CH_2O), 1.17 (s, 6H, CCH_3), 0.67 (s, 6H, CCH_3). ^{13}C{^{1}H} NMR ($CDCl_3$): δ 211.00 (*cis* *C*O, aq, $|^2J(PC) + {}^2J(PC')|$ 30 Hz), 206.39 (*trans* *C*O, t, $|^2J(PC)|$ 13 Hz), 167.76 (s, *C*=O), 75.35 (s, *C*H), 73.85 (s, *C*H_2O), 73.08 (s, *C*H_2O), 53.17 (s,O*C*H_3), 31.33 (s, *C*CH_3), 22.41

Table 4
Selected bond lengths (Å) and bond angles (°) for compounds **4, 5, 7**.

	4	5	7
M–P(1)	2.192(3)	2.2184(17)	2.198(3)
M–P(2)	2.191(2)	2.2145(16)	2.244(3)
O(1)–P(1)	1.598(7)	1.604(4)	1.595(9)
O(2)–P(2)	1.605(6)	1.609(4)	1.604(8)
C(1)–O(1)	1.443(11)	1.440(7)	1.430(15)
C(1)–C(2)	1.511(13)	1.520(8)	1.508(17)
C(2)–O(2)	1.444(11)	1.446(7)	1.447(14)
M–Cl(1)	2.328(3)	2.3190(16)	2.330(3)
M–Cl(2)	2.339(3)	2.3281(17)	2.323(4)
P(1)–M–P(2)	95.57(9)	95.31(6)	98.35(12)
O(1)–P(1)–M	116.8(3)	116.69(16)	115.7(3)
C(1)–O(1)–P(1)	128.2(6)	128.0(4)	119.3(8)
O(1)–C(1)–C(2)	106.6(7)	106.9(4)	105.1(10)
O(2)–C(2)–C(1)	107.4(7)	105.9(4)	110.2(9)
C(2)–O(2)–P(2)	128.2(6)	129.0(4)	129.0(8)
O(2)–P(2)–M	117.4(2)	116.85(16)	122.1(3)
C(3)–C(1)–C(2)	114.7(8)	114.5(5)	115.0(11)
C(4)–C(2)–C(1)	113.1(9)	112.5(5)	113.2(12)
Cl(1)–M–P(1)	175.22(10)	175.19(6)	174.35(13)
Cl(2)–M–P(1)	88.76(10)	87.73(6)	83.27(13)
Cl(1)–M–P(2)	87.25(10)	86.17(6)	86.96(12)
Cl(2)–M–P(2)	171.82(10)	171.60(7)	178.06(14)
Cl(1)–M–Cl(2)	88.93(11)	91.44(7)	91.45(13)

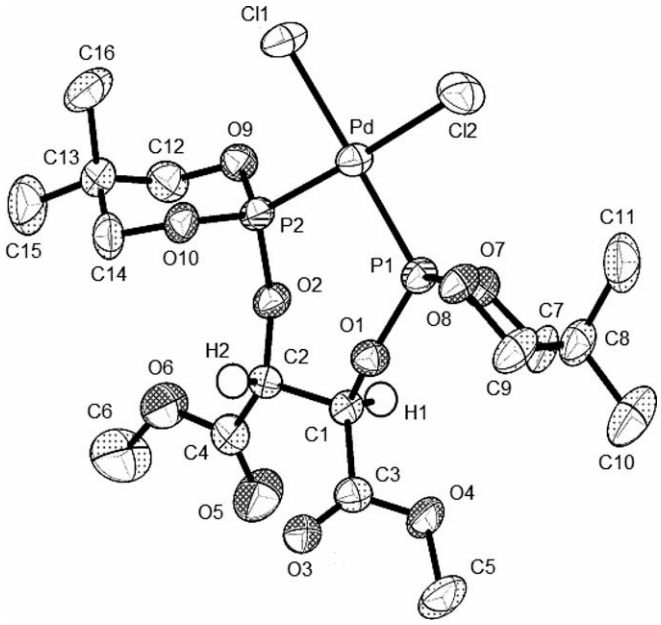

Fig. 3. ORTEP [19] drawing of the molecular structure of **5**. Thermal ellipsoids are drawn at the 50% probability level and hydrogens in calculated positions are omitted for clarity.

(s, C*C*H_3), 22.37 (s, C*C*H_3). IR (CH_2Cl_2): ν(cm^{-1}) 2046 m, 1957 sh, 1934 s.

*cis-PtCl$_2$(**1**) (**4**).* To a 100 mL round bottom flask was added 0.190 g (0.508 mmol) of $PtCl_2$(cod) and 50 mL of degassed CH_2Cl_2. This solution was stirred until all of the $PtCl_2$(cod) had dissolved at which time 0.225 g (0.508 mmol) of **1** was added in one portion. The reaction mixture was stirred for 30 min resulting in a slightly pale yellow solution. A ^{31}P{^{1}H}NMR spectrum of the reaction mixture was then taken and exhibited the single resonance of the product. The mixture was evaporated to dryness under aspirator vacuum, and the residue placed on the pump to insure removal of all excess cyclooctadiene and solvent to yield 0.129 g (90.8%) of crude **4** as a white solid. The crude product was recrystallized from CH_2Cl_2/hexanes to yield colorless X-ray quality crystals. Anal. Calc. for $C_{16}H_{28}O_{10}Cl_2P_2Pt$: C, 27.13; H, 3.98. Found: 26.93; H, 3.88%. ^{31}P NMR ($CDCl_3$): δ 66.12. (s with ^{195}Pt satellites, $|^1J(Pt-P)|$ = 2948 Hz) ^{1}H NMR ($CDCl_3$): δ 5.28 (dd, 2 H, $|^2J(PH)|$ 7.1 Hz, $|^3J(HH)|$ 2.3 Hz C*H*), 4.26 (m, 4H, CH_2O), 3.98 (m, 4H, CH_2O), 3.89 (s, 6H, OCH_3), 1.45 (s, 6H, CCH_3), 0.90 (s, 6H, CCH_3). ^{13}C{^{1}H} NMR ($CDCl_3$): δ 166.10 (s, *C*=O), 76.61 (s, *C*H), 75.90 (s, *C*H_2O), 75.11 (s, *C*H_2O), 53.65 (s, O*C*H_3), 33.27 (s, *C*CH_3), 21.98 (s, C*C*H_3), 21.87 (s, C*C*H_3) (see Fig. 4).

*cis-PdCl$_2$(**1**) (**5**).* To a 100 mL round bottom flask was added 0.075 g (0.423 mmol) of $PdCl_2$ and 50 mL of degassed CH_2Cl_2. This solution was allowed to stir overnight to ensure that all $PdCl_2$ had dissolved, at which time 0.187 g (0.423 mmol) of **1** was added in one portion. The pale orange reaction mixture was stirred for 30 min resulting in a slightly pale yellow solution. A ^{31}P{^{1}H}NMR spectrum of the reaction mixture was then taken and exhibited the single resonance of the product. The mixture was evaporated to dryness under aspirator vacuum, and the residue was placed on the pump to insure removal of all excess solvent to yield 0.253 g (96.6%) of crude **5** as a pale yellow solid. The crude product was recrystallized from CH_2Cl_2/hexanes resulting in pale yellow X-ray quality crystals. Anal. Calc. for $C_{16}H_{28}O_{10}Cl_2P_2Pd$: C, 31.01; H, 4.55. Found: 31.02; H, 4.53%. ^{31}P{^{1}H} NMR ($CDCl_3$): δ 89.82 (s). ^{1}H NMR ($CDCl_3$): δ 5.16 (dd, 2H, $|^2J(PH)|$ 7.1 Hz, $|^3J(HH)|$ 2.3 Hz C*H*), 4.35 (m, 4H, CH_2O), 3.82 (m, 4H, CH_2O), 3.76 (s, 6H, OCH_3),

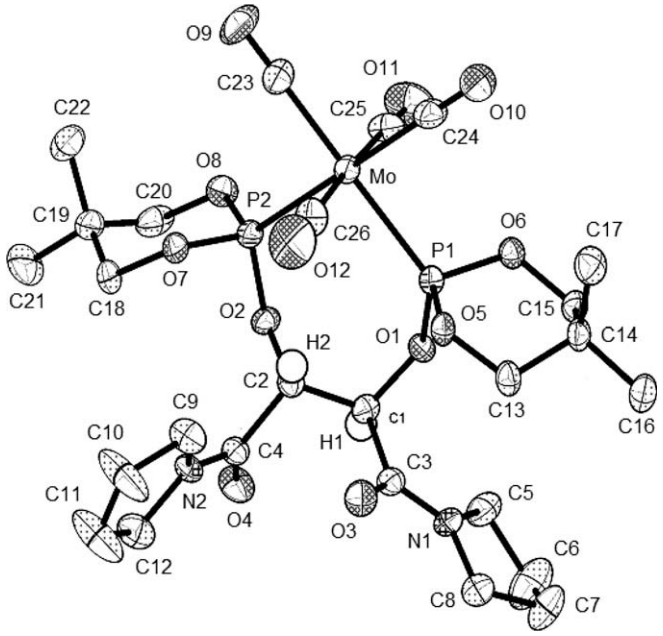

Fig. 4. ORTEP [19] drawing of the molecular structure of **6**. Thermal ellipsoids are drawn at the 50% probability level and hydrogens in calculated positions are omitted for clarity.

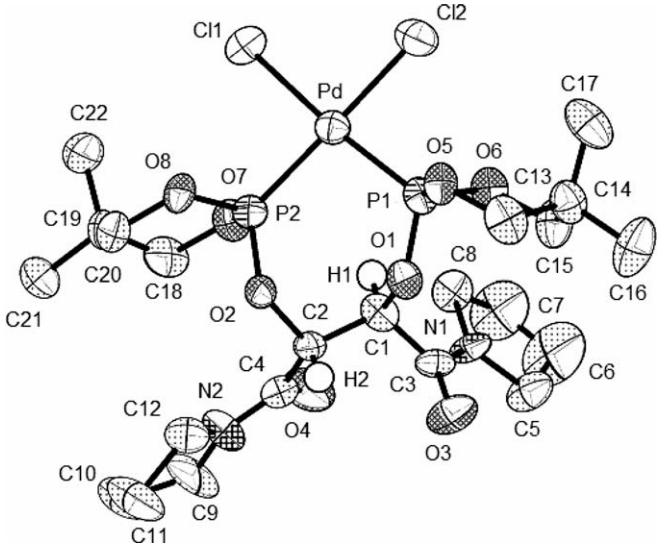

Fig. 5. ORTEP [19] drawing of the molecular structure of **7**. Thermal ellipsoids are drawn at the 50% probability level and hydrogens in calculated positions are omitted for clarity.

1.09 (s, 6H, CCH_3), 0.87 (s, 6H, CCH_3). $^{13}C\{^1H\}$ NMR ($CDCl_3$): δ 167.92 (s, *C*=O), 75.27 (s, *C*H), 73.89 (s, *C*H_2O), 72.94 (s, *C*H_2O), 52.38 (s,O*C*H_3), 31.44 (s, *C*CH_3), 21.81 (s, C*C*H_3), 21.69 (s, C*C*H_3).

*cis-Mo(CO)$_4$(**2**) (**6**).* Following the procedure for **3**, 0.288 g (0.960 mmol) of $Mo(CO)_4$(nbd) and 0.500 g (0.960 mmol) of **2** gave 0.651 g (93.1%) of crude **6** as a white solid. The crude product was recrystallized from CH_2Cl_2/hexanes to yield colorless X-ray quality crystals. Anal. Calc. for $C_{26}H_{38}N_2O_{12}P_2Mo$: C, 41.06; H, 5.04. Found: 40.98; H, 5.02%. ^{31}P NMR ($CDCl_3$): δ 154.54 (s). ^1H NMR ($CDCl_3$): δ 5.51 (dd, 2H, $|^3J(HH)|$ 7.5 Hz, $|^3J(PH)|$ 7.5 Hz C*H*), 3.95 (t, 4H, $|^4J(HH)|$ 2.8 Hz, CH_2O), 3.74 (t, 4H, $|^4J(HH)|$ 2.8 Hz, CH_2O), 3.45 (m, 8H, CH_2N), 1.91 (m, 8H, CH_2C), 1.30 (s, 6H, CH_3C), 0.73 (s, 6H, CH_3C). $^{13}C\{^1H\}$ NMR ($CDCl_3$): δ 210.88 (*trans* *C*O, dd, $|^2J(PC) + {}^2J(PC')|$ 30 Hz), 206.33 (*cis* *C*O, t, $|^2J(PC)|$ 13 Hz), 165.88 (s, *C*=O), 73.25 (s, *C*H_2O), 73.11 (s, *C*H), 72.37 (s, *C*H_2O) 46.38 (s, *C*H_2N), 45.78 (s, *C*H_2N), 32.11 (s, *C*CH_3), 26.11 (s, *C*H_2C), 24.35 (s, *C*H_2C) 22.12 (s, C*C*H_3), 22.00 (s, C*C*H_3) (see Fig. 5).

*cis-PdCl$_2$(**2**) (**7**).* Following the procedure for **5**, 0.075 g (0.42 mmol) of $PdCl_2$ and 0.22 g (0.42 mmol) of **2** gave 0.28 g (96%) of crude **7** as a pale yellow solid. The crude product was recrystallized from CH_2Cl_2/hexanes to yield pale yellow X-ray quality crystals. Anal. Calc. for $C_{22}H_{38}O_8N_2Cl_2P_2Pd$: C, 37.81; H, 5.49. Found: 37.65; H, 5.44%. ^{31}P NMR ($CDCl_3$): δ 90.97. ^1H NMR ($CDCl_3$): δ 5.03 (dd, 2H, $|^3J(HH)|$ 7.5 Hz, $|^3J(PH)|$ 7.5 Hz C*H*), 3.64 (t, 4H, $|^4J(HH)|$ 2.8 Hz, CH_2O), 3.58 (t, 4H, $|^4J(HH)|$ 2.8 Hz, CH_2O), 3.24 (m, 8H, CH_2N), 1.85 (m, 8H, CH_2C), 1.07 (s, 6H, CH_3C), 0.92 (s, 6H, CH_3C). $^{13}C\{^1H\}$ NMR ($CDCl_3$): δ 167.58 (s, *C*=O), 73.86 (s, *C*H_2O), 73.49 (s, *C*H), 72.77 (s, *C*H_2O) 46.42 (s, *C*H_2N), 45.88 (s, *C*H_2N), 33.01 (s, *C*CH_3), 26.94 (s, *C*H_2C), 24.67 (s, *C*H_2C) 22.18 (s, C*C*H_3), 22.07 (s, C*C*H_3).

3. Results and discussion

3.1. Syntheses and NMR spectroscopic characterization

The phosphite ligands **1** and **2** were synthesized by the reactions of the appropriate diols with the 2-chloro-5,5-dimethyl-1,3,2-dioxaphosphorinane in the presence of Et_3N with THF as the solvent (Scheme 1). Both reactions yielded the respective bis(phosphite) ligands in near quantitative yields as white solids. The ligands were deemed pure and used in subsequent reactions only if there were no extraneous resonances in the ^{31}P, ^1H, and ^{13}C NMR spectra.

The transition metal complexes were prepared by reacting the appropriate metal precursor complex and the ligand in CH_2Cl_2 (Scheme 2). These reactions gave nearly quantitative yields of the complexes upon evaporation of the reaction solvents, and analytically pure, X-ray quality crystals were obtained by recrystallization of each complex from a dichloromethane/hexanes mixture.

The ligands and complexes were characterized in solution using multinuclear NMR spectroscopy. Each ligand and complex exhibited a single ^{31}P NMR resonance. The chemical shifts of the ^{31}P NMR resonances of the *cis*-$Mo(CO)_4$L complexes (154.68 ppm for **3** and 154.54 ppm for **6**) were similar to that of a closely related complex (151.8 ppm) in which the bridging group is derived from *o*-catechol rather than a tartrate ester [12]. The chemical shifts of the ^{31}P NMR resonances of the *cis*-$Mo(CO)_4$(ligand) complexes are also similar to those previously reported for the *cis*-$Mo(CO)_4${R-OP($OCH_2CMe_2CH_2O$)}$_2$ (R = alkyl or aryl) [13] complexes (151.22–154.99 ppm) even though the ligands in this complexes are monodentate.

There have been no literature reports of *cis*-$PdCl_2$L complexes similar to those in this study, but Nifant'ev et al. [14] have reported a *cis*-$PtCl_2L_2$ complex with monodentate phosphite ligands that is very closely related to those in this study. The chemical shifts of the ^{31}P NMR resonances in Nifant'ev's complex with two inequivalent phosphites (63.8 and 64.2 ppm) are similar to that of *cis*-$PtCl_2$(**1**) (**4**, 66.12 ppm).

The similarities of the chemical shifts of the ^{31}P NMR resonances of the complexes in this study with those of complexes with related monodentate ligands suggest that ring strain is not significant in the seven-membered chelated rings in the complexes in this study. To further investigate this observation, the ^{31}P NMR coordination chemical shifts ($\Delta\delta$) of the complexes in this study have been compared to those of related complexes. Those of the *cis*-$Mo(CO)_4$L complexes have been compared to those for two complexes with monodentate phosphite ligands (*cis*-$Mo(CO)_4$(2,2′-$C_{12}H_8O_2$)POR)$_2$: R = Me (**8**), $\Delta\delta$ = 33.06 ppm [15];

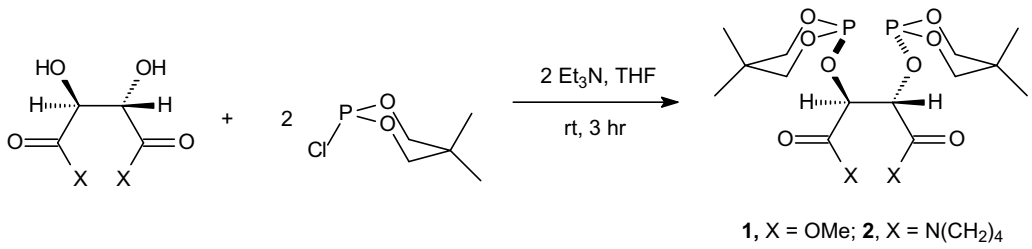

Scheme 1. Synthesis of ligands **1** and **2**.

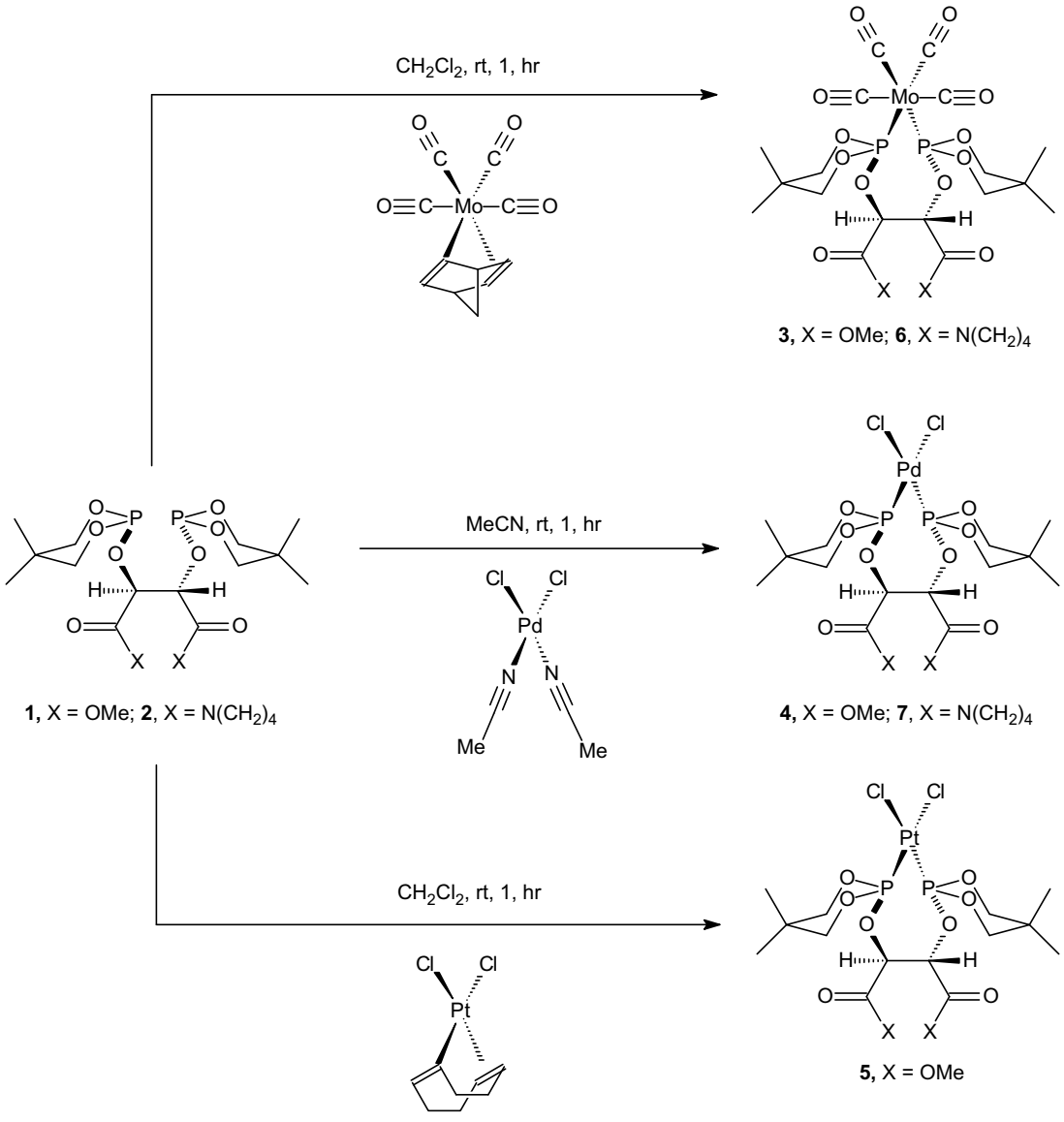

Scheme 2. Syntheses of metal complexes of **1** and **2**.

R = OCH_2CH_2OEt (**9**), $\Delta\delta$ = 30.47 ppm [15]) and for a complex with a long chain bis(phosphite) ligands (*cis*-$Mo(CO)_4${(2,2′-$C_{12}H_8O_2$)$PO(CH_2CH_2O)_4P$(2,2′-$C_{12}H_8O_2$)} (**10**), $\Delta\delta$ = 29.70 ppm) [16]. The coordination chemical shifts for the *cis*-$PtCl_2$(**1**) complex (**4**, −57.07 ppm) and the *cis*-$PdCl_2L$ complexes (L = **1** (**5**), −33.32 ppm; L = **2** (**7**); −33.06 ppm) were compared to those of similar complexes of the monodentate (2,2′-$C_{12}H_8O_2$)$POCH_2CH_2OEt$ ligand, (*cis*-$PtCl_2L_2$ (**11**), −54.10 ppm; *cis*-$PdCl_2L_2$ (**12**), −30.09 ppm) [15]. The fact that similar coordination chemical shifts are seen for complexes with the same metal centers, regardless of the ligand that is used, strongly suggests that the seven member rings in the tartaric acid-derived ligands in this study, **1** and **2**, experience no significant ring strain when they cis coordinate to transition metal centers.

Table 5
Torsion angles (°) for the seven-membered chelate rings in **3–7.**

Compound	C–C–O–P	O–P–M–P	M–P–O–C	O–C–C–O
$Mo(CO)_4L_{(1)}$ (**3**)	−96.4 (4)	−21.05 (14)	90.6 (3)	72.3 (5)
	−97.2 (4)	−29.19 (14)	86.1 (3)	
$PtCl_2L_{(1)}$ (**4**)	−94.6 (9)	−18.4 (3)	89.8 (7)	69.3 (9)
	−98.0 (8)	−29.4 (3)	84.2 (7)	
$PdCl_2L_{(1)}$ (**5**)	−96.1 (5)	−18.18 (19)	89.4 (4)	69.9 (5)
	−99.4 (5)	−28.77 (18)	85.5 (4)	
$Mo(CO)_4L_{(2)}$ (**6**)	37.6 (10)	−3.3 (3)	−71.7 (6)	62.1 (8)
	−118.0 (6)	20.9 (3)	55.6 (6)	
$PdCl_2L_{(2)}$ (**7**)	37.7 (14)	4.4 (5)	−68.0 (10)	69.3 (9)

3.2. Crystallographic studies

The X-ray crystal structures of complexes **3–7** have been determined to gain a better understanding of the coordination chemistry of ligands **1** and **2** in the solid state. Of particular interest are the effects of the substituents on the tartrate backbone (ester in **1** versus amide in **2**) on the conformations of the seven-membered chelate rings. The torsion angle data in Table 5 and the deviations from a least-squares plane through the seven-membered chelate rings in Table 6 clearly demonstrate that the conformation of the ring changes significantly when the tartrate backbone is changed, but that it is unaffected when the metal center is changed from *cis*-octahedral to *cis*-square planar or when the metal is changed from Pd(II) to Pt(II). These data suggest that the conformational changes are not simply related to solid state interactions, but rather that changing the tartrate substituents changes the low energy conformation of the seven-membered chelate ring (see Table 7).

The conformations of the seven-membered chelate rings in the *cis*-$Mo(CO)_4$(**1**) (**3**), and *cis*-$Mo(CO)_4$(**2**) (**6**), complexes are shown in Fig. 6. The conformation of the chelate ring in **3** has nearly twofold symmetry about an axis running from the Mo through the center of the tartrate C–C bond. In contrast, the chelate ring conformation in **6** is more of an envelope conformation with Mo, P1, P2, O1 and O2 forming the body and C1 and C2 the flap. Given that the conformation is not affected by the nature of the metal center and thus not due to crystal packing forces, as discussed in the previous paragraph, the mostly likely explanation for the different conformations of the chelate rings is that the ring conformation is very sensitive to the steric bulk of the tartrate substituents.

The fact that the conformations in the seven-membered chelate rings in ligands **1** and **2** are different suggests that coordination geometries of the complexes could exhibit different deviations from the idealized octahedral and square planar geometries. Selected bond angles around the metal centers are listed in Tables 3 and 4. These data clearly demonstrate that the complexes of ligand **1** (which has ester substituents) have smaller angles than do those of ligand **2** (which has amide substituents) (for: **3**, 89.83° (4), versus **6**, 93.53°(7), for *cis*-MCl_2L: 95.57° (9), **4**, and 95.31°(6), **5**, versus 98.35°(12), **7**). The fact that the complexes of ligand **2** have larger angles suggests that the larger substituents on the tartramide backbone lead to a larger bite angle upon chelation to the metal center. The very different P–M–P bond angles of ligands **1** and **2** are consistent with the different average cis P–Mo–C angles in the two *cis*-$Mo(CO)_4L$ complexes (**3**: 90.26(37)° and **6**: 88.4°(9)).

The above data suggest that ligand **2** behaves as if it is considerably more bulky than is ligand **1** even though both ligands form seven-membered chelate rings and both ligands have identical phosphorus substituents. This conclusion is supported by comparing the P–M–P bond angles in **3** and **6** to those in other *cis*-$M(CO)_4$(phosphite)$_2$ complexes. A complex with monodentate phosphite ligands, *cis*-$Mo(CO)_4$(2,2′-$C_{12}H_8O_2POCH_3)_2$ (**13**) [17], has a P–Mo–P angle of 87.23(7)° that is smaller than that of **3** even though the phosphorus substituents are considerably larger. The metallacrown ether complex, *cis*-$Mo(CO)_4${(2,2′-$C_{12}H_8O_2$)PO($CH_2CH_2O)_4$P(2,2′-$C_{12}H_8O_2$)} (**10**), has the same phosphorus substituents as does **13**, but has a larger a P–Mo–P angle of 91.21(3)° probably due to the long chelate chain connecting the two phosphites. This angle is somewhat larger than is the P–Mo–P angle in **3**, but considerably smaller than is the P–Mo–P angle in **6**. These comparisons suggest that varying the tartrate substituents on ligands such as **1** and **2** is a facile method for controlling the steric bulk and the bite angle of the ligand.

Although the conformation of the seven-membered chelate ring is sensitive to the nature of the tartrate substituents, the conformations of the 6-membered 1,3,2-dioxaphosphorinane rings (defined by the least squared planes through the phosphorus and two oxygens (OPO), through the two oxygens and two methylene carbons (O_2C_2) and through the two methylene carbons and the methyne carbon (C_3)) are not (Table 8). In every case, the 1,3,2-dioxaphos-

Table 6
Deviations from least squares plane and dihedral angles for complexes **3–7**.

	Atom	$Mo(CO)_4L_{(1)}$ (**3**)	$PtCl_2L_{(1)}$ (**4**)	$PdCl_2L_{(1)}$ (**5**)	$Mo(CO)_4L_{(2)}$ (**6**)	$PdCl_2L_{(2)}$ (**7**)
Deviations from least squares plane through chelate ring	M	0.0466	0.0525	0.0500	0.1488	0.2278
	P1	−0.2856	−0.2670	−0.2589	−0.1708	−0.2278
	P2	0.2119	0.1884	0.1841	0.1715	0.1191
	O1	0.4018	0.3797	0.3831	−0.4800	−0.3765
	O2	−0.4240	−0.3996	−0.3979	−0.3551	−0.4807
	C1	−0.1928	−0.2064	−0.2166	0.0362	0.0543
	C2	0.2420	0.2524	0.2561	0.6507	0.6873
Dihedral angle (°)[a]		24.74	24.12	23.90	9.45	8.16

[a] Dihedral angle is defined by the angle between the plane through P–M–P and the plane through O–centroid–O, where the centroid is the middle of the C(1)–C(2) bond.

Table 7
Dihedral angles in the 1,3,2-dioxaphosphorinane rings in complexes **3–7**.

Dihedral Angle(°)[a]	$Mo(CO)_4L_{(1)}$ (**3**) [°]	$PtCl_2L_{(1)}$ (**4**) [°]	$PdCl_2L_{(1)}$ (**5**) [°]	$Mo(CO)_4L_{(2)}$ (**6**) [°]	$PdCl_2L_{(2)}$ (**7**) [°]
Ring 1					
Plane 1 and Plane 2	51.21	50.73	50.33	50.96	52.09
Plane 2 and Plane 3	35.08	34.52	35.18	37.47	37.91
Plane 1 and Plane 3	16.16	16.26	15.20	13.49	14.18
Ring 2					
Plane 1 and Plane 2	53.12	51.95	53.38	53.28	49.52
Plane 2 and Plane 3	34.34	36.29	35.67	31.56	35.95
Plane 1 and Plane 3	18.81	15.74	17.79	21.74	13.60

[a] Dihedral angle is defined by the angle between the designated plane. Plane1 is through the C–C–C of the chair. Plane 2 is through the O–C–C–O of the chair. Plane 3 is through the O–P–O of the chair.

Table 8
Average Mo–C and C–O distances (Å) for the carbonyl ligands in **3** and **6**.

Bond	**3**	**6**
Mo–C (*trans*) [a]	2.006(8)	2.023(13)
Mo–C (*cis*)[b]	2.037(8)	2.032(21)
C–O (*trans*)[a]	1.147(8)	1.130(14)
C–O (*cis*)[b]	1.128(8)	1.132(20)

[a] Carbonyls *trans* to one of the phosphites.
[b] Carbonyls *cis* to both of the phosphites.

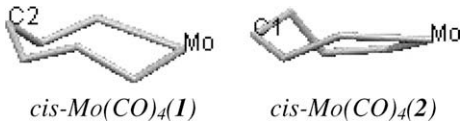

*cis-Mo(CO)$_4$(**1**)* *cis-Mo(CO)$_4$(**2**)*

Fig. 6. Conformations of the seven-membered chelate rings in complexes **3** and **6**.

phorinane rings are distorted chairs in which the angle between the OPO plane and the O_2C_2 plane is considerably less than the ideal angle of 60° and the angle between the O_2C_2 plane and the C_3 plane is close to the ideal angle of 60°. This conservation of the chair conformation is a common feature of 1,3,2-dioxaphosphorinane ligands [18].

The C–O and Mo–C bond distances in *cis*-Mo(CO)$_4$L complexes can provide insight into the σ-donor/π-acceptor abilities in the phosphorus-donor ligands [18]. The average C–O and Mo–C bond distances for **3** and **6** are given in Table 8. As expected there is an inverse correlation between the C–O and Mo–C distances for **3** indicating that the phosphite is a better σ-donor/poorer π-acceptor than is a carbonyl ligand. This inverse correlation is not seen for **6**. This is likely due to distortions in the carbonyl coordination geometry due to crystal packing forces in **6**.

4. Conclusions

In summary, two new chiral bis(phosphite) ligands and five transition metal complexes containing these ligands have been synthesized, and the structures determined by X-ray crystallography. These studies demonstrate that tartaric acid derivatives are excellent building blocks for the synthesis of these chiral bis(phosphite) ligands. Further, it appears that the solid state conformations of the seven-membered chelate rings in these complexes are sensitive to the nature of the tartrate substituents. If this is also the case in solution, changes in the backbone substituents of the tartrate could result in changes in catalytic activities and selectivities of transition metal complexes of these types of ligands.

Supplementary material

CCDC 691447, 691448, 691449, 691450 and 691451 contain the supplementary crystallographic data for this paper. These data can be obtained free of charge from The Cambridge Crystallographic Data Centre via www.ccdc.cam.ac.uk/data_request/cif.

Acknowledgments

We would like to thank the Department of Chemistry at the University of Alabama at Birmingham for their support through a graduate fellowship. We would also like to thank The Center for Optical Sciences and Spectroscopies (COSS) for additional funding.

References

[1] H.B. Kagan, T.P. Dang, J. Chem. Soc., D: Chem. Commun. (1971) 481.
[2] G.J.H. Buisman, P.C.J. Kamer, P.W.N.M. van Leeuwen, Tetrahedron: Asymmetr. 4 (1993) 1625–1634.
[3] T.J. Kwok, D.J. Wink, Organometallics 12 (1993) 1954–1959.
[4] M. Suzuki, Y. Kimura, S. Terashima, Bull. Chem. Soc. Jpn. 59 (1986) 3559–3572.
[5] J.G. Verkade, D.W. White, R.D. Bertrand, G.K. McEwen, J. Am. Chem. Soc. 92 (1970) 7125–7135.
[6] H.C. Clark, L.E. Manzer, J. Organomet. Chem. 59 (1973) 411–428.
[7] D.C. Smith Jr., G.M. Gray, Inorg. Chem. 37 (1998) 1791.
[8] W. Ehrl, R. Rinck, H. Vahrenkamp, J. Organomet. Chem. 56 (1973) 285.
[9] A. Varshney, G.M. Gray, Inorg. Chem. 30 (1991) 1748–1754.
[10] CAD4-PC Ver. 1.2, Enraf Nonius, Delft, The Netherlands, 1988.
[11] G.M. Sheldrick, SHELXTL6.1, Bruker AXS, Madison, WI, 2000.
[12] A.C. Dros, A. Meetsma, R.M. Kellogg, Tetrahedron 55 (1999) 3071–3090.
[13] G.M. Gray, W. Watt, J. Organomet. Chem. 434 (1992) 181–199.
[14] E.E. Nifant'ev, M.P. Koroteev, G.Z. Kaziev, A.M. Koroteev, L.K. Vasyanina, I.S. Zakharova, Russ. J. Gen. Chem. 73 (2003) 1686–1690.
[15] A.A. Kaisare, S.B. Owens Jr., G.M. Gray, unpublished results.
[16] J.M. Butler, G.M. Gray, J.P. Claude, Polyhedron 23 (2004) 1719–1729.
[17] H. Byrd, J.D. Harden, J.M. Butler, M.J. Jablonsky, G.M. Gray, Organometallics 22 (2003) 4198–4205.
[18] J.M. Butler, T.E. Knight, S. Sotoudehnia, P.D. Kadle, S.L. Green, G.M. Gray, J. Chem. Crystallogr. 34 (2004) 111–118.
[19] M.N. Burnett, C.K. Johnson, ORTEP-III: Oak Ridge Thermal Ellipsoid Plot Program for Crystal Structure Illustrations, Oak Ridge National Laboratory Report ORNL-6895, 1996.